

# Influence of nano- and micro-roughness on vortex generations of mixing flows in a cavity

**Okulov, V. L.; Sharifullin, B. R.; Okulova, N.; Kafka, J.; Taboryski, R.; Sørensen, J. N.; Naumov, I. V.**

*Published in:*
Physics of Fluids

*Link to article, DOI:*
10.1063/5.0083503

*Publication date:*
2022

*Document Version*
Publisher's PDF, also known as Version of record

# Influence of nano- and micro-roughness on vortex generations of mixing flows in a cavity

Cite as: Phys. Fluids **34**, 032005 (2022); https://doi.org/10.1063/5.0083503
Submitted: 27 December 2021 • Accepted: 20 February 2022 • Published Online: 04 March 2022

V. L. Okulov, B. R. Sharifullin, N. Okulova, et al.

Physics of Fluids ARTICLE scitation.org/journal/phf

# Influence of nano- and micro-roughness on vortex generations of mixing flows in a cavity

Cite as: Phys. Fluids **34**, 032005 (2022); doi: 10.1063/5.0083503
Submitted: 27 December 2021 · Accepted: 20 February 2022 ·
Published Online: 4 March 2022



V. L. Okulov,[1,2,a] B. R. Sharifullin,[2] N. Okulova,[3] J. Kafka,[3] R. Taboryski,[4] J. N. Sørensen,[1] and I. V. Naumov[2]

## AFFILIATIONS

[1]Department of Wind Energy, Technical University of Denmark, Kgs. Lyngby, 2800, Denmark
[2]Institute of Thermophysics, SB RAS, Novosibirsk, 630090, Russian Federation
[3]Inmold A/S, Savsvinget 4B, Horsholm, DK-2970, Denmark
[4]DTU Nanolab, Technical University of Denmark, Kgs. Lyngby, DK-2800, Denmark

**Note:** This paper is part of the special topic, Kitchen Flows.
[a]**Author to whom correspondence should be addressed:** vokulov@mail.ru

## ABSTRACT

Experiments were carried out in a water-filled elongated cup of a "kitchen scale," where motion was created by a rotating disk with various micro- and nano-roughness in the top of the cup. The obtained results have shown that for some patterns of nanostructures, there is a noticeable growth of a vortex, generated by the disk, while other roughnesses do not make visible changes in the flow structure. The results are of interest in assessing the efficiency of surfaces with nanoscale roughnesses. Indeed, the first type of nano-roughness may become useful for enhancing soft mixing in chemical and bio-reactors, including in the preparation of special food delicacies. On the other hand, the use of nanostructured surfaces that do not affect the main flow can help to solve some industrial problems of water and ice erosion, for example, in wind turbines or any other objects where disturbances of the main flow are undesirable.



## I. INTRODUCTION

Among the many solutions of nature to increase the intensity of liquid flows, perhaps the most unexpected is the use of surfaces with different roughnesses. The largest roughnesses are humps of the humpback whale, being prototypes of vortex generators.[1,2] The medium-sized roughness is shark skin—a prototype of ribbed walls.[3] The effectiveness of the smallest ones discovered on the lotus surface[4] (in this article, it is referred to as a nanoscale roughness) has not yet been investigated carefully.

There are many examples of laminar or turbulence flow regimes where the useful impact of the different roughnesses was discovered, e.g., in jets, wakes, or pipe flows in which the small or large coherent vortex structures were periodically or chaotically generated by such rough surfaces.[5–8] Unfortunately, for all mentioned complex flow cases, it usually becomes impossible to separate and estimate a pure impact of the roughness only on one flow component, e.g., the vortex formation, because the feedback mechanism of different flow instabilities usually is present. The dynamic interactions with other coherent structures in the flows should strongly influence the growth of vorticity over any rough walls, too. It remains even more important how to get a clear understanding and practice using the aerodynamic impact of the roughness on the growth vorticity without including the influence of other flow properties, such as the development instability, drag effects, etc. Therefore, several modifications of the roughness with different micro or nanoscales need to be studied separately to estimate their real impact and to choose different modifications of the small roughness in modern technologies correctly.

In the current investigation, we will try to formulate and solve only one problem of the complex flows, which is governed by the vorticity generation on a rough wall without or with an infinitesimal influence of the disturbances in the flow. As it was noted above, our particular interest is to study the generation and growth of stationary vorticity inflows over rough walls.

Further development of some applications requires knowledge regarding the pure influence of the different micro-/nano-scale roughnesses including their hierarchical structures on the growth of the initial macro-vortex. In this regard, the main objective of the article is to assess the impact of micro-/nano-scale roughness on the macro-size of

a stable vortex produced in stable confined cavity flows in a water-filled elongated cup. In addition to establishing general knowledge about the effect of nano-roughness on the vorticity generation, the current study of swirling flows in a cavity is of special applied importance for improving heat and mass transfer processes in chemical, biological, and energy technologies using vortex cavities for mixing.[9] Indeed, in recent years, many industries, such as medicine, microbiology, pharmaceutical, petrochemical industries, etc., require soft but effective mixing of liquids, including those with variable viscosity, without the formation of foam, water hammer, cavitation, high-turbulence, and stagnant zones.[10,11]

From the point of view of the use of vortex mixing technologies for Kitchen Flows in contrast to traditional mixing devices with mechanical or magnetic stirrers, this is mainly to ensure gentle (non-traumatic) mixing of bio cultures beneficial to the body during the formation of various yogurts, creams, healthy, or baby meals. In the gentle mixing mode, due to the organization of the vortex movement not with a mechanical stirrer but a rotating disk without blades, when the foam is not formed, useful bio cultures are not destroyed at the cellular level, thus increasing the "usefulness" of the manufactured product and the concentration of living microorganisms.

In this paper, we describe an experiment to demonstrate the impact of hierarchical micro-/nano-roughness on the formation of macro-vortex structures. The paper is organized as follows. In Sec. II, we describe the experimental setup and the measurement method. Section III describes the structures of the roughness investigated here. In Sec. IV, we describe the experimental results to demonstrate the influence of nano- or micro-disturbances of cavity surface on the growth of the macro-vortex structure. Finally, in Sec. V, we discuss the results to conclude the work in Sec. VI.

## II. EXPERIMENTAL SETUP AND METHOD

Many fundamental problems (vortex breakdown, velocity jump, reversal flow, counterflow slip, etc.) were investigated with the help of swirling flow in a cylindrical cavity.[12–15] In our study, we will also use this conventional setup, shown in Fig. 1, with a high cylinder to test the stable vortex cell generated by the rotating top end wall. The container has a radius $R = 47$ mm and a height $h = 10R$, and $L$ denotes the axial length of the rotating vortex cell, which is schematically shown in the figure under the rotating disk of the top end wall. The container was filled with a 66% aqueous solution of glycerin. The density and kinematic viscosity were 1170 kg/m$^3$ and 11.3 mm$^2$/s at a temperature of 22.6 °C, respectively. The vortex motion in the fluid cell under the top end wall was generated by a disk of the same radius, which rotated with an angular velocity $\omega$, while the other walls of the container were stationary. The disk rotation was produced by a stepper motor. Centrifugal force affects the fluid in the cylinder when the disk rotates, forcing the fluid to flow out along the top end wall from the axis to the disk periphery. Then, the fluid descends downward along the walls of the cylinder, down to a length of size L, where it turns again and converges to the axis, forming a central vortex with an ascending flow at the axis forming the vortex cell (circular arrows indicate the direction of flow in the cell in Fig. 1). The intensity of the fluid motion is described by the Reynolds number $Re = \omega R^2/\nu$, where $\nu$ is the kinematic viscosity of the working fluid. The temperature was controlled during the experiment. The temperature changed by no more than 0.3 °C. In this case, a change in temperature by 1 °C gives a small experimental error of about 2% for the angular velocity of disk rotation $\omega$ at $Re = 2000$.

The fluid is put into motion by rotating the top lid using a stepper motor with a precision of 1/750 rotation per second (RPS). For the present setup and working fluid, a Reynolds number of 1000 corresponds to about 1 RPS. Thus, for the range of Re considered, the variation in angular velocity during a revolution is less than 0.14%. As the viscosity of the working fluid is very sensitive to temperature changes, the viscosity/temperature relation was carefully controlled during the experiments. The fluid temperature was controlled within 0.1 °C, leading to an uncertainty of 0.4% for the viscosity. The total error of Re did not exceed ±30 in a range of Reynolds numbers from 1000 to 10 000.

In the experiment, we used an MC023MG-SY Ximea CMOS camera (resolution—2.3 MP 1936 × 1216, shooting frequency—165

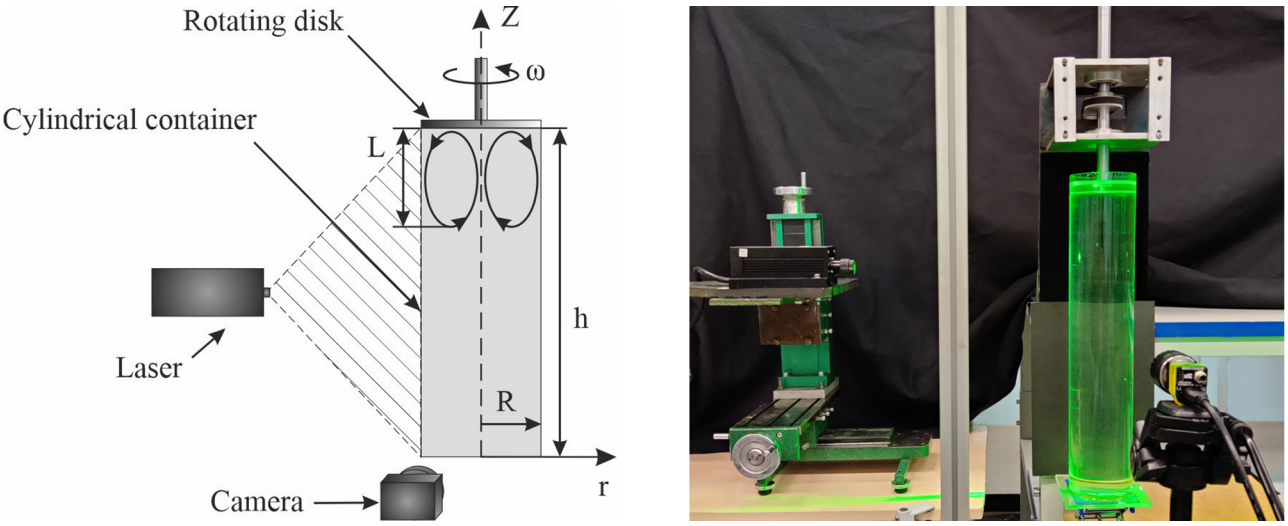


**FIG. 1.** Scheme of the flow with vortex cell and photo of the setup.

fps, matrix—Sony IMX174 LLJ-C) with a Nikon AF Nikkor 28 mm f/2.8D lens. To increase the measurement accuracy, the camera was installed opposite the boundary of the circulation cell, and the length of the region falling on the matrix was 166 mm, which made it possible to obtain images with a high spatial resolution of 11 pix/mm. The length of the circulation cell was measured with an accuracy of 1 mm, which provided an error of no more than 0.8%. Thus, the total error in the formation of a vortex flow and measurement of a vortex cell at the worst combination is determined by summing all the components of the error: $0.8\% + 0.4\% + 0.14\% \leq 1.5\%$, which is less than the effects recorded and considered in the article, which amount to 5%–10%.

Investigations of an evolution of the vortex cell were carried out in a vertical section, passing through the axis of the cylinder. The cylindrical wall in the setup was made from optical grade plexiglass to use contactless optical methods successfully. Accurate measurements of the velocity field are required to establish the kinematic characteristics of growth in the size $L$ of the vortex cell (Fig. 1); however, the accuracy of modern particle image velocimetry (PIV) is not sufficient to study a rapidly decaying vortex, where the velocity on the axis decreases exponentially with a decrease in the distance from the rotating disk and very quickly tends to zero.[16,17] Since the velocities of fluid movement in the measurement region are small, the flow is certainly laminar. For this reason, a long-term visualization for a more accurate determination of the vortex boundary was therefore used.[11,18] Small local Reynolds numbers corresponding to flow with very low velocities on the stationary boundary without pulsations permitted recording of a visual picture of the flow quite well. The flow visualization by a laser light knife with a thickness of 1 mm in the central cross-section of the cylinder was used to study the topology of the vortex cell. Polyamide particles of neutral buoyancy with an average diameter of 10 $\mu$m were used as light-scattering additives. Figure 2 depicts an example of a track visualization showing the formation of an upward reversal flow along the cylinder axis in the vortex cell and the boundary between the cell and immobile flow in the cylinder. The boundary between the cell flow and immobile fluids indicates the length $L$ of the vortex cell.

In our experiments, the length $L$ of the vortex cell was determined visually from the images of the track system in the vertical cross section, when the tracks indicate the boundary of the flow motion converging to the axis from the periphery under immobile fluids. The image processing algorithm of Ref. 18 is used to improve the quality of flow visualization, for which a series of fixed-mode photographs were averaged. The background image was subtracted from the averaged image. Further, during image processing, a two-dimensional high-frequency filter and linear amplitude correlation were used. It should be noted that the superhydrophobic properties of surfaces are usually studied when air is trapped between nanostructures—the Cassie-Baxter effect[19]—but this regime is unstable, and the gas layer is for many reasons destroyed, and in most cases, the Wenzel regime prevails.[20] In this work, the flow studies were carried out in the absence of an air gap between the liquid and the surface. To establish the lifetime of the air gap until its complete disappearance from the rough surface of the disk, two methods of reaching the tested steady-state rotation modes were investigated. In the first case (short test 1), the disk began to rotate immediately when it was placed in the cavity, while still retaining air bubbles between its roughness and the liquid in the cavity. In the second case (long test 2), first, the disk placed in the cavity rotated for a long time to eliminate air bubbles due to centrifugal force, then it stopped, remaining completely in the liquid, and then after a pause of 10 minutes, it began to rotate at the same speed as in the first test. Figure 3 for the regime at $\mathrm{Re} = 750$ shows the differences between the two tests. The initial size $L$ after the start of disk rotation is smaller (square symbols). Both tests converge to the same vortex size $L$ after 4 min when all the entrapped air has left the nanostructures.

The angular velocity $\omega$ of the disk rotation at each Reynolds number and the dimensionless time required for the flow to stabilize at the maximum depth of the vortex cell are shown in Table I. In the

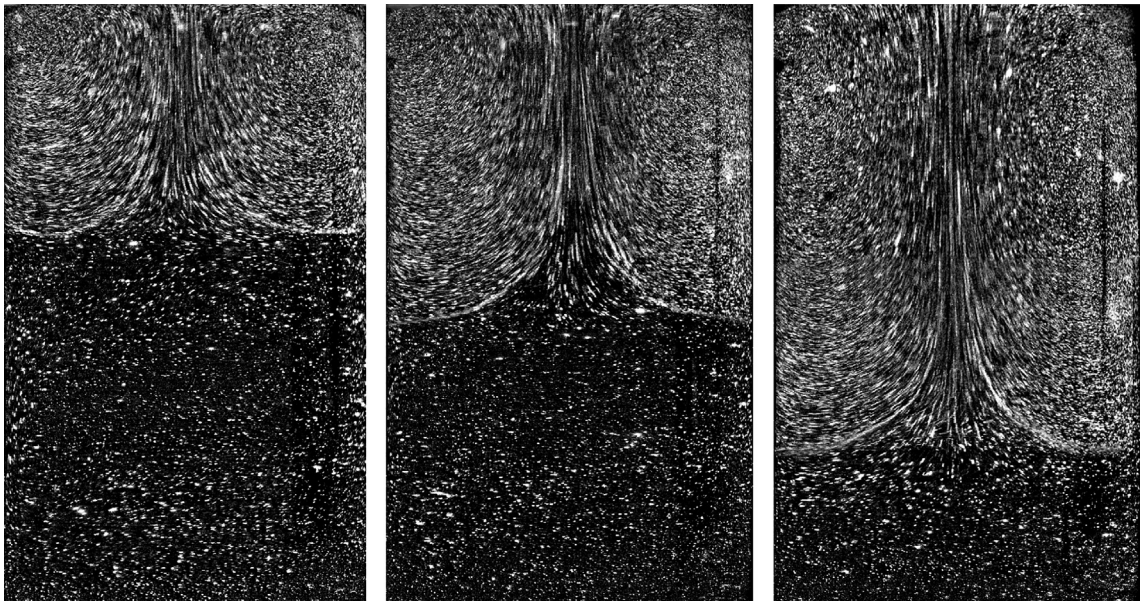

**FIG. 2.** Examples of flow visualizations in the cylinder at $\mathrm{Re} = 100$, 250, and 500.

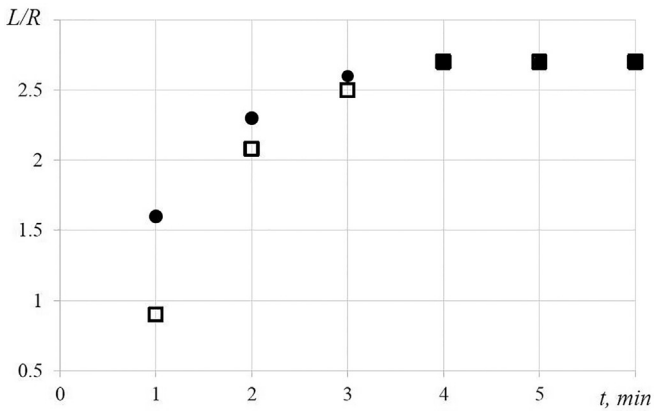


**FIG. 3.** Length of vortex structure as a function of time to reach the stationary regime at Re = 750 for cases with (□—test 1) and without (●—test 2) air on the disk surface.

experiments to be shown in the following, measurements were made 15 minutes after starting the angular rotation of the disk because the maximum time to stabilize the flow takes up to 10 minutes, depending on the Reynolds number.

## III. SURFACE ROUGHNESS

The prototypes of the nano-roughness surface in this study are superhydrophobic surfaces, which are usually used for their water-repellent properties. Their water-repellent properties are based on the preservation of the "air sheet," i.e., air bubbles keep between the nano- or micro-roughnesses. A prototype of such a structure in nature is the self-cleaning superhydrophobic lotus leaf surface.[21] Since the 1990s, the lotus effect has been carefully studied[22] to know a topography from micro to the nanoscale, for which air is captured between the surface texture and the liquid lying on top (i.e., the Cassie or Cassie-Baxter state). Over the years, an infinite number of examples of structures resembling superhydrophobic surfaces with hierarchical roughness have been published[23] with numerous examples of successful and efficient use of superhydrophobic coatings in energy and transport, e.g., the hydrophobic properties can be used to prevent water and ice erosion on turbine blades.[24] However, there is a serious problem with superhydrophobic surfaces, since the liquid on the rough substrate can also exist in the Wenzel state[20] when water completely displaces the air to wet the substrate. In other words, the hydrophobic effect is lost when air is completely displaced by working fluid. The Wenzel's case corresponds to a simple streamlining of surfaces with very small roughness, and it still has no practical value.

In this study, we attempted to identify the usefulness of nanostructured surfaces in the case of complete displacement of the "air sheet" with working fluid. The effectiveness of the smallest roughness for the vortex generation has not yet been investigated in the cavity flows.

Successful biomimetic surfaces are still not used in many engineering solutions due to the high production cost. The recent achievements in the field of mass-production of micro- and nano-roughness[25] opened up the possibility of studying the interaction of these surface structures in different fluid flows. For this task, it is planned to use lithographic micro- and nano-textured surfaces produced using fast and cheap roll-to-roll (R2R)-EC technology to create nanostructures from 50 nanometers to 100 $\mu$m in size on polymer films.[26–29]

A total of five different surface structures imprinted in polypropylene (PP) films were examined and compared to an unstructured smooth film or a natural roughness (a replica of a polished silicon wafer with atomic surface smoothness). The shown surface structures are various combinations of three main structures: nanograss, micro-grooves, and some combinations of nanograss with micro-grooves (Fig. 4).

Micro-grooves were created using photolithography. Silicon wafers were coated with photoresist and illuminated with UV light. The photoresist was then used as a soft mask in a deep-reactive ion-etching (DRIE) process, the so-called Bosch process, where numerous steps of etching and passivation were repeated to obtain a straight sidewall etched into the silicon wafer. This method creates a wavy sidewall with structures called scallops. The size of each scallop achieved in this process was approximately 150 nm. After the etching process, the soft mask was removed using oxygen plasma. Structures S8, S9, S10, and S14 were made using one or two consecutive steps of photolithography.

The so-called nanograss pattern was obtained using alternating aggressive and passivating gases, $SF6 + CH_4$ and $O_2$, respectively. By varying the flow rates of the two gas mixtures, different morphologies were obtained, forming a needlelike pattern, also referred to as back silicon. The wafers were etched at −10 °C for 8 min. Samples S6, S8, and S9 were etched using the described process (S8 and S9 after the photolithography step).

The produced structures were replicated in polypropylene using the R2R EC process, as described in Ref. 25.

**TABLE I.** The minimum time for the flow stabilization.

| Re | $\omega$, rad/s | Dimensionless time, $\omega$T |
|---|---|---|
| 250 | 1.52 | 145 |
| 500 | 3.03 | 174 |
| 750 | 4.55 | 217 |
| 1000 | 6.06 | 290 |
| 1250 | 7.58 | 290 |
| 1500 | 9.09 | 347 |
| 1750 | 10.61 | 406 |
| 2000 | 12.12 | 463 |

## IV. EXPERIMENTAL RESULTS AND DISCUSSION

A series of experiments were carried out in a cylindrical container with an upper rotating disk ($R = 47$ mm and $h = 470$ mm) with smooth and rough surfaces. An experimental study was carried out to study how the various roughness morphologies (Fig. 4) on the surface of the rotating disk influence the change of the vortex-cell growth $L/R$ [Fig. 1(a)].

First, for further comparisons, a propagation of the swirl into the cavity depth was measured for cases without roughness: the Plexiglas disk without polymer films (S—case) and the disk with a smooth polymer film (S0—case). Figure 5 shows the curves for the growth of the vortex cell for a smooth Plexiglas disk and a disk with a film without roughness (symbols). It can be seen that there is no difference between these cases. The solid curve in Fig. 5 shows an approximation of the dependence on Re of the maximum axial length L of the cell adjacent

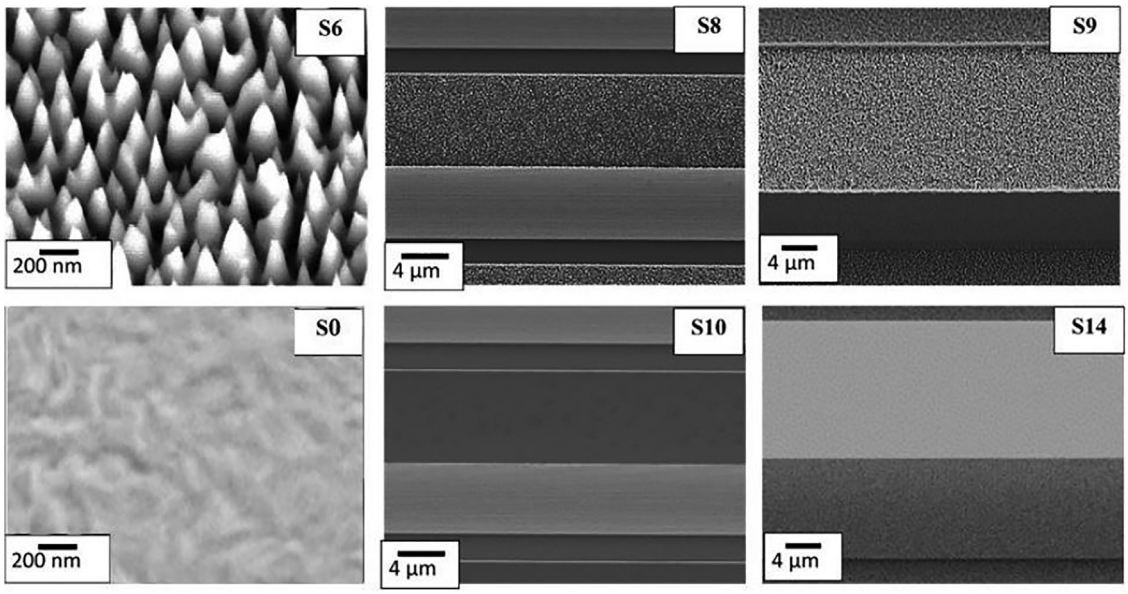


| ID | Structure type |
|---|---|
| S6 | Nanograss |
| S0 | Natural roughness |

| ID | Structure type |
|---|---|
| S8 | 10 μm lines + Nanograss |
| S10 | 10 μm lines |

| ID | Structure type |
|---|---|
| S9 | 20 μm lines + Nanograss |
| S14 | 20 μm lines |

**FIG. 4.** Overview of the different master structures used in the investigations.

to the rotating disk. Here, this dependence is presented as a simple function of the angular velocity of the disk rotation,

$$L \propto 2\pi R\sqrt{\omega R} \text{ or in dimensionless form } L/R = 0.0975R\sqrt{\omega/\nu}. \quad (1)$$

We note that this implies a proportionality $L \propto \sqrt{Re}$. The simple curve (1) and the experimental symbols come together with good accuracy in almost the entire range of $Re$ variation in the tests.

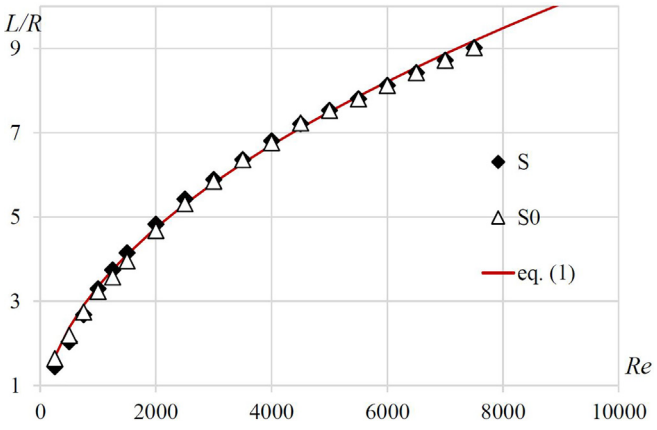


**FIG. 5.** Growth of the vortex cell into the depth of the cylindrical cavity with the smooth disk.

Next, the disk covered by films of different macro and nanostructures in Fig. 4 was examined. Figure 6 shows the dependences of the length of the vortex cell as a function of $Re$ for all types of roughness.

Analyzing the data obtained in the experiments, in Fig. 6, all the roughnesses were divided into two groups:

**Group 1 (G1)**: films of S10 and S14, where the growth of the vortex cell is the same as compared with the smooth film of Fig. 5, described by curve (1);
**Group 2 (G2)**: films S6, S8, and S9, providing the maximum increase in the size of the vortex cell in comparison with a smooth film.

G1 includes different combinations of the micro-lines only, whereas G2 comprises the nanograss surface (S6), two combinations of the micro-lines with the nano-grass (S8, S9). The main difference between the groups is that the roughness in G2 comprises nanograss elements resulting in pronounced vortex growth.

The measurements of the disks with the roughness of 2G are well approximated by the curves,

$$L \propto 2\pi R\sqrt{1.12\omega R} \text{ or in dimensionless form } L/R = 0.0975R\sqrt{1.12\omega/\nu}. \quad (2)$$

For the second group, the same growth of vortex cells is also observed, which correlates well with Eq. (2), indicating the strong macro impact (about $R$ or 50 mm) of nanostructures (with very small-size of 150 nm) of the coatings S6, S8, and S9 with the roughness on the development of the swirling flow. It should be noted that the macro difference of the sizes of the vortex-cells is experimentally well-distinguishable

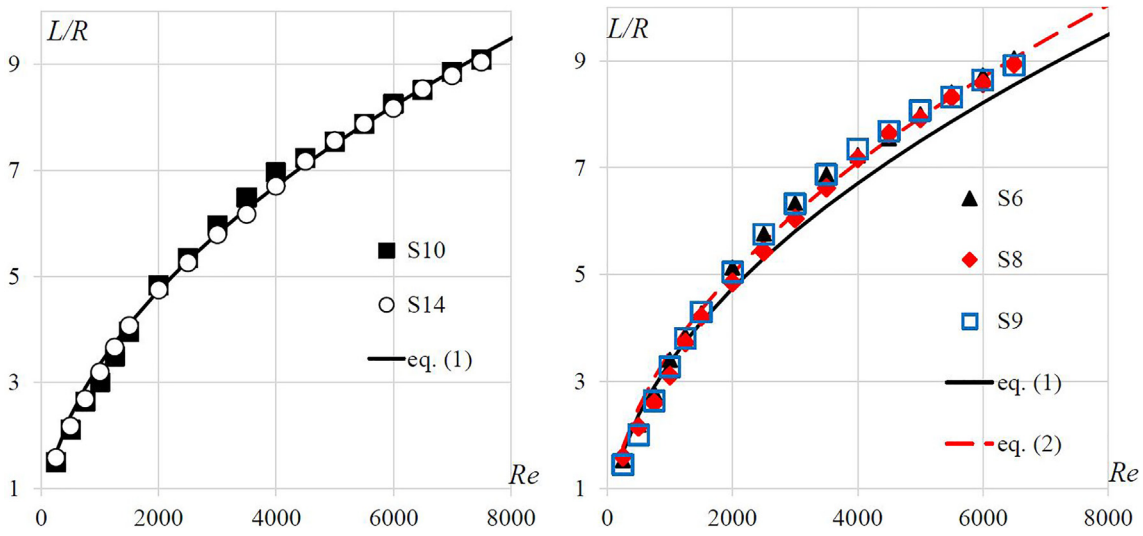


**FIG. 6.** Growth of a vortex cell into the depth of the cylinder for the tested types of films.

about 0.6 R at large Re like the growth shown in Fig. 2, which points out the minimal effect of random errors. It should also be mentioned that according to Eq. (2), the tendency for the vortex cell to grow deeper for all types of nanoscale surface reliefs from the second group corresponds to a generated increase in the flow swirl by 12%.

In an additional investigation, some comparisons between velocities at different flow locations were performed for the disk with the natural roughness (S0) and the nano-grass (S6) to confirm the cell growth. At different Reynolds numbers, the axial velocity component ($V_z$) was measured by laser Doppler anemometry (LDA) near the rotating disk at 0.1 R–1 R of vertical distances under the disk and at the flow axis ($r = 0$) and for radial distance with maximal velocity ($r/R = 0.85$) where velocity magnitude has significant value. The LDA (LAD-06i) using a Mitsubishi ML1013R semiconductor laser (with 70 mW power and 684 nm wavelength) and operating a backscattering configuration was made at the Kutateladze Institute of Thermophysics SB RAS.[30] The system has been well tested in many experimental studies of rotating flows. The LDA history was recorded for 120 seconds with the rate of 400 LDA samples per second, which was sufficient for determining the mean velocity.

Table II shows the comparisons obtained from experimental data for different points ($r/R$, $z/R$) from the rotating disk and Reynolds numbers. According to this measurement, it is possible to see that for all cases, axial velocity for S6 is slightly more than for S0. These differences are about 1%–3%.

Since the growth of the vortex structure is associated with an energy balance of the flow, it needs to make this comparison through quantities proportional to the energy characteristics, that is, the squares of the velocities,

$$\Delta V_z^2 = \frac{V_z(S6)^2 - V_z(S0)^2}{V_z(S0)^2} * 100\%. \quad (3)$$

Table III shows the relative changes in the squares of the speed in percent, calculated by the formula (3). One can be seen that the values increase for all cases of downstream removal from the rotating disk,

**TABLE II.** The axial velocity at different locations in cavity flow.

| Points | | *Vz*, mm/s | | | | | | | |
|---|---|---|---|---|---|---|---|---|---|
| *r/R* | *z/R* | Re = 250 | | Re = 500 | | Re = 1000 | | Re = 1500 | |
| 0 | 0.1 | 2.37 | 2.51 | 4.97 | 5.26 | 5.69 | 6.12 | 7.68 | 8.12 |
| | 0.2 | 4.02 | 4.11 | 7.87 | 8.39 | 8.75 | 9.45 | 11.6 | 12.1 |
| | 0.5 | 4.82 | 4.87 | 11.6 | 11.9 | 16.1 | 16.5 | 18.6 | 18.9 |
| | 1 | 1.87 | 1.89 | 8.42 | 8.53 | 16.7 | 17.3 | 24.2 | 24.6 |
| 0.85 | 0.1 | −4.45 | −4.45 | −16.6 | −18.1 | −25.8 | −26.1 | −34.8 | −36.4 |
| | 0.2 | −5.51 | −5.51 | −12.5 | −12.7 | −22.3 | −23.1 | −28.6 | −29.7 |
| | 0.5 | −3.16 | −3.17 | −7.5 | −7.51 | −13.9 | −14.5 | −18.5 | −18.9 |
| | 1 | −0.78 | −0.81 | −3.4 | −3.49 | −7.98 | −8.37 | −12.3 | −12.9 |

**TABLE III.** Relative axial velocity squares at different locations in cavity flow.

| Points | | $\Delta V_z^2$, % | | | |
|---|---|---|---|---|---|
| $r/R$ | $z/R$ | Re = 250 | Re = 500 | Re = 1000 | Re = 1500 |
| 0 | 0.1 | 12.2 | 12 | 15.1 | 11.8 |
| | 0.2 | 4.5 | 13.6 | 16.4 | 8.7 |
| | 0.5 | 1.7 | 5.2 | 5.1 | 3.3 |
| | 1 | 2.2 | 2.6 | 7.3 | 3.4 |
| 0.85 | 0.1 | 0 | 15.8 | 2.5 | 8.6 |
| | 0.2 | 1.8 | 3.3 | 6.8 | 7.3 |
| | 0.5 | 0.6 | 1.3 | 8.1 | 4.2 |
| | 1 | 7.3 | 5.6 | 9.1 | 9.1 |

which is about 5%–10% at Re > 1000, which corresponds to and explains the increase in vortex cell size shown in Fig. 6.

## V. DISCUSSION

Recently, many features on the influence of micro- and nano-inhomogeneities on the macroscopic properties of vortex formation in flows have been reported. In particular, studies published recently in this journal[31,32] have established macroscopic changes in vortex structures (centimeter scale) when a small amount of $SiO_2$-nanotubes are added to a de-ionized liquid in a flow behind a step or when a 50 $\mu$m "hair" coating is added on the wall of a streamlined cylinder. Based on the macro-characteristics of the flow, the authors of Ref. 31 concluded that adding a small amount of $SiO_2$ nanofluid in the water had a significant effect on the turbulence generation of the flow. Likewise, the authors of Ref. 32 concluded that the micro "hair" coating on the leeward side of a cylinder surface leads to a significant change of the vortex formation. These observations corroborate the existence of a connection between the macro-characteristics of the vorticity in the flows and microscopic perturbations of the liquid-solid interface (the concentration of nanotubes or the length and position of the "hair" coating). However, in the above-mentioned studies, only quantitative effects are reported, and no explanation or theoretical description of the observed phenomena is offered. The problem is that the big difference in scales between the nanostructures and the characteristic length scale of the flow not easily can explain the observed differences using "classical" macro-physics energy balance, and so far it has only been possible to measure and report, but not to explain, the observed phenomena.

In the present study, a significant influence of nanocoatings on the macroscopic size of a stationary vortex structure in a closed swirling flow is reported. Various geometries and azimuthal sizes of nanocoatings were investigated to identify the possible cause of this phenomenon. We found no effect of azimuthal micro-scale roughness of the coating on the increase in vortex macrostructure size with angular velocity (or Re number). The additional vortex growth, when compared to the smooth reference sample, was observed only for coatings comprising nano-grass. For structures with other azimuthal dimensions, the macro-vortex did not increase more in size than for the original smooth wall reference. In contrast to the experiments of Ref. 31 described above, we believe that the stationary nature of the flow indicates that the vortex growth is not due to an intensification of turbulent characteristics. This hypothesis is indirectly confirmed by the constant azimuthal size of the nanostructure, at which the macro-vortex grows, and previously discovered numerically and experimentally resonant properties of swirling limited flows.

Indeed, the swirling flow in a closed cylindrical container with a rotating lid has been the subject of numerous experimental and computational studies for more than 50 years. The wide interest in this configuration was triggered by experiments of Escudier[33] that described the unusual topology of these closed flows. His work was followed by dozens of experimental and numerical studies, which found more and more interesting features in this closed swirling flow. In particular, in numerical linear analysis of the propagation of axisymmetric and azimuthal infinitesimal perturbations in the cavity, exponentially growing marginal and critical modes were found for cylinders of aspect ratios up to 5.5 for a wide range of Reynolds numbers.[34,35] The existence of marginal and critical modes was revealed in numerical calculations[32,33] and confirmed by experiments,[36] but with a background level of perturbations, which, due to the natural roughness of the cavity walls, is smaller than that of the nano-grass shown in this work. Figure 4, with micrographs of S0 and S6, compares the nano-grass (S6) and the natural roughness of the disk (S0). Subsequently, the existence of exponentially growing modes was discovered, especially in the case of multiple cellular flows appearing in cylinders with high aspect ratios.[16,17] The experimental study in Ref. 18 only contains a single vortex cell near the rotating lid, which initiated our interest for cell growth due to disk roughness as a result of the exponentially growing marginal and critical modes found in calculations.[17]

The special size of roughness can be explained by the existence of the corresponding exponentially increasing axisymmetric modes in which the cell growth is observed. This means that the size of the nanograss most closely corresponds to the critical mode of the growth of axisymmetric perturbations in the closed cavity. Other sizes of roughness do not influence the growth of the vortex cell and do not produce the critical modes.

## VI. CONCLUSION

The possibility of intensifying the mass transfer in a closed cylindrical container filled with liquid was investigated using a rotating end wall (disk) with various types of different macro- and nanostructures on its surface. The rotation of the disk is transmitted to the container and forms an annular vortex cell, which propagates into the depth of the cylinder when the angular velocity of disk-rotation increases. The experiments were carried out to measure the axial growth of a vortex cell at different angular velocities of the disk rotation or with the associated Reynolds number.

The growth of the vortex cell for different roughnesses of the micro and nano sizes was compared with the data for the smooth disk. For the convenience of the comparison, a dependence of the growth of the vortex cell has been established as a function of the square root from the angular velocity of the disk.

Different combinations of three basic elements were investigated as roughness: nanograss, micro-grooves, and some combinations of nanograss with micro-lines. A significant increase in the size of the vortex cell was found for the roughness containing the nano-grass. The relationship between the growth of the cell size and the roughness size was first established. The discovered maximal effect for the disk with the nanograss was a 12% increase in the angular velocity for the rotation in comparison to the smooth disk. All larger microstructures did not significantly affect the growth of the vortex cell for the current tests.

These results are of interest for evaluating the efficiency of using surfaces with nano-roughness in closed swirling flows. In particular, it can be used to develop vortex technologies when creating more intensive mixing in vortex bio and chemical reactors and in vortex mixing technologies for Kitchen Flows. Of additional interest is the detection of nanostructures whose presence does not affect the main flow. This fact requires further careful consideration and investigation, since such structures, while maintaining their hydrophobic properties, may not affect the performance of, for example, wind turbines.

## ACKNOWLEDGMENTS

The analysis and approximation of Wenzel's states in the cavity flows were funded by Russian Science Foundation under Grant No. 21-19-00205, and all experiments in the flow were performed under the state contract with IT SB RAS.

## AUTHOR DECLARATIONS

### Conflict of Interest

The authors declare no conflict of interests.

## DATA AVAILABILITY

The data that support the findings of this study are available within the article.

## NOMENCLATURE

| | |
|---|---|
| DRIE | deep-reactive ion-etching |
| $h$ | container height (mm) |
| $L$ | axial length of the vortex cell (mm) |
| $R$ | container radius (mm) |
| Re | Reynolds number (–) |
| UV | ultraviolet |
| $\nu$ | kinematic viscosity of working liquid ($mm^2/s$) |
| $\rho$ | fluid densities ($kg/m^3$) |
| $\omega$ | angular velocity of lid rotation (rad/s) |
| °C | Gradus Celsius |

## REFERENCES

[1]E. Kadivar, M. V. Timoshevskiy, M. Y. Nichik, O. el Moctar, T. E. Schellin, and K. S. Pervunin, "Control of unsteady partial cavitation and cloud cavitation in marine engineering and hydraulic systems," Phys. Fluids **32**, 052108 (2020).
[2]C. M. Velte, M. O. L. Hansen, and V. L. Okulov, "Multiple vortex structures in the wake of a rectangular winglet in ground effect," Exp. Therm. Fluid Sci. **72**, 31–39 (2016).
[3]X. Pu, G. Li, and H. Huang, "Preparation, anti-biofouling and drag-reduction properties of a biomimetic shark skin surface," Biol. Open **5**(4), 389–396 (2016).
[4]J. Jimenez, "Turbulent flows over rough walls," Ann. Rev. Fluid Mech. **36**, 173–196 (2004).
[5]B. Forouzi Feshalami, S. He, F. Scarano, L. Gan, and C. Morton, "A review of experiments on stationary bluff body wakes," Phys. Fluids **34**, 011301 (2022).
[6]A. Dhamanekar and K. Srinivasan, "Effect of impingement surface roughness on the noise from impinging jets," Phys. Fluids **26**, 036101 (2014).
[7]M. Toloui, A. Abraham, and J. Hong, "Experimental investigation of turbulent flow over surfaces of rigid and flexible roughness," Exp. Therm. Fluid Sci. **101**, 263–275 (2019).
[8]O. A. B. Saleh, "Fully developed turbulent smooth and rough channel and pipe flows," Ph.D. thesis, Erlangen-Nürnberg University, 2005.
[9]V. N. Shtern, *Cellular Flows* (Cambridge University Press, New York, 2018), p. 573.
[10]L. K. Nielsen, "Bioreactors for hematopoietic cell culture," Annu. Rev. Biomed. Eng. **1**, 129 (1999).
[11]S. G. Skripkin, B. R. Sharifullin, I. V. Naumov, and V. N. Shtern, "Dual vortex breakdown in a two-fluid whirlpool," Sci. Rep. **11**, 23085 (2021).
[12]I. V. Naumov, S. G. Skripkin, and V. N. Shtern, "Counterflow slip in a two-fluid whirlpool," Phys. Fluids **33**, 061705 (2021).
[13]J. N. Sørensen, I. V. Naumov, and V. L. Okulov, "Multiple helical modes of vortex breakdown," J. Fluid Mech. **683**, 430–441 (2011).
[14]I. V. Naumov, B. R. Sharifullin, A. Y. Kravtsova, and V. N. Shtern, "Velocity jumps and the Moffatt eddy in two-fluid swirling flows," Exp. Therm. Fluid Sci. **116**, 110116 (2020).
[15]I. V. Naumov, B. R. Sharifullin, M. A. Tsoy, and V. N. Shtern, "Dual vortex breakdown in a two-fluid confined flow," Phys. Fluids **32**(6), 061706 (2020).
[16]C. P. Hills, "Eddies induced in cylindrical containers by a rotating end wall," Phys. Fluids **13**, 2279 (2001).
[17]M. A. Herrada, V. N. Shtern, and M. M. Torregrosa, "The instability nature of Vogel-Escudier flow," J. Fluid Mech. **766**, 590 (2015).
[18]B. R. Sharifullin and I. V. Naumov, "Angular momentum transfer across the interface of two immiscible liquids," Thermophys. Aeromech. **28**, 65 (2021).
[19]A. B. D. Cassie, "Contact angles," Discuss. Faraday Soc. **3**, 11–16 (1948).
[20]R. N. Wenzel, "Resistance of solid surfaces to wetting by water," Ind. Eng. Chem. **28**(8), 988–994 (1936).
[21]W. Barthlott and C. Neinhuis, "Purity of the sacred lotus, or escape from contamination in biological surfaces," Planta **202**(1), 1–8 (1997).
[22]M. Ma and R. M. Hill, "Superhydrophobic surfaces," Curr. Opin. Colloid Interface Sci. **11**(4), 193–202 (2006).
[23]E. Søgaard, N. K. Andersen, K. Smistrup, S. T. Larsen, L. Sun, and R. Taboryski, "Study of transitions between wetting states on microcavity arrays by optical transmission microscopy," Langmuir **30**(43), 12960–12968 (2014).
[24]V. Okulov, I. Kabardin, D. Mukhin, K. Stepanov, and N. Okulova, "Physical de-icing techniques for wind turbine blades," Energies **14**(20), 6750 (2021).
[25]B. N. Sahoo and B. Kandasubramanian, "Recent progress in fabrication and characterisation of hierarchical biomimetic superhydrophobic structures," RSC Adv. **4**(42), 22053–22093 (2014).
[26]N. Okulova, "Industrial-scale pattern transfer using roll-to-roll extrusion coating: Understanding the process and exploring its applications," Ph.D. thesis, Technical University of Denmark, 2018.
[27]S. Murthy, M. Matschuk, Q. Huang, N. K. Mandsberg, N. A. Feidenhans'l, P. Johansen, L. Christensen, H. Pranov, G. Kofod, H. C. Pedersen, O. Hassager, and R. Taboryski, "Fabrication of nanostructures by roll-to-roll extrusion coating," Adv. Eng. Mater. **18**(4), 484–489 (2016).
[28]A. Telecka, S. Murthy, L. Schneider, H. Pranov, and R. Taboryski, "Superhydrophobic properties of nanotextured polypropylene foils fabricated by roll-to-roll extrusion coating," ACS Macro Lett. **5**, 1034–1038 (2016).
[29]N. Okulova, P. Johansen, L. Christensen, and R. Taboryski, "Replication of microsized pillars in polypropylene using the extrusion coating process," MEE **176**, 54–57 (2017).
[30]I. V. Naumov, B. R. Sharifullin, and M. A. Tsoy, "Experimentally investigating the instability onset in closed polygonal containers," Exp. Fluids **60**, 178 (2019).
[31]J. Lv, C. Hu, M. Bai, L. Li, L. Shi, and D. Gao, "Visualization of $SiO_2$-water nanofluid flow characteristics in backwardfacing step using PIV," Exp. Therm. Fluid Sci. **101**, 151 (2019).
[32]M. Hasegawa and H. Sakaue, "Experimental investigation of aerodynamic drag and flow characteristics of circular cylinder with microfiber coating," Exp. Therm. Fluid Sci. **129**, 110478 (2021).
[33]M. P. Escudier, "Observations of the flow produced in a cylindrical container by a rotating endwall," Exp. Fluids **2**, 189 (1984).
[34]A. Gelfgat, P. Z. Bar- Yoseph, and A. Solan, "Three-dimensional instability of axisymmetric flow in rotating lid-cylinder enclosure," J. Fluid Mech. **438**, 363 (2001).
[35]A. Gelfgat, "Three-dimensional instability of axisymmetric flows: Solution of benchmark problems by a low-order finite volume method," Int. J. Numer. Methods Fluids **54**, 269 (2007).
[36]J. N. Sørensen, A. Gelfgat, I. Naumov, and R. Mikkelsen, "Experimental investigation in three-dimensional flow instabilities in a rotating lid-driven cavity," Phys. Fluids **21**, 054102 (2009).